



Article

Microstructure of Mortar with Ballast Waste as a Cement Replacement

Santiago Yagüe-García ¹ and Rosario García-Giménez ²,* ©

- Departamento de Ingeniería Industrial, Facultad de Ingeniería, Avenida de la Universidad, Villanueva de la Cañada, 6, 28691 Madrid, Spain; syagugar@uax.es
- Departamento de Geología y Geoquímica, Facultad de Ciencias, Universidad Autónoma de Madrid, 28049 Madrid, Spain
- * Correspondence: rosario.garcia@uam.es or rosario.garcia@alumni.uam.es

Abstract: The use of ballast in tracks generates waste that, in most cases, is destined for landfill. The proposal to use this waste as a replacement in OPC in different proportions valorizes the waste and allows its participation in the Circular Economy. To this end, two samples of ballast waste with substitution ratios (10, 15, and 20%) were studied for one year using pozzolanic activity, XRD, SEM/EDX, and CT scanning analysis. The shortest setting times corresponded to the ballast waste substitutions with the highest percentage, which is related to particle size and the presence of amorphous material, thereby reducing the setting time. The workability of mortars with a substitution indicates that the average consistency decreases as the substitution percentage increases, while the loss of fluidity grows with a higher substitution percentage. Porosity is linked to the formation of C-S-H gels and the presence of ettringite, which fills the pores between particles. Tortuosity can be considered low, which hinders the transport of aqueous solutions, making the substituted cements studied more resistant to hydration processes.

Keywords: CDW ballast; pozzolanic reaction; supplementary cementitious material; porosity



Academic Editor: Muhammad Junaid Munir

Received: 28 March 2025 Revised: 27 April 2025 Accepted: 15 May 2025 Published: 16 May 2025

Citation: Yagüe-García, S.; García-Giménez, R. Microstructure of Mortar with Ballast Waste as a Cement Replacement. *Appl. Sci.* **2025**, *15*, 5605. https://doi.org/10.3390/app15105605

Copyright: © 2025 by the authors. Licensee MDPI, Basel, Switzerland. This article is an open access article distributed under the terms and conditions of the Creative Commons Attribution (CC BY) license (https://creativecommons.org/licenses/by/4.0/).

1. Introduction

The utilization of construction and demolition waste produced in cement manufacturing is one of the challenges facing modern society. One of the least well-known types of waste is that generated after the useful life of ballast, which serves as a substrate for railway tracks.

The design and operation of railway systems must comply with both technical and legal requirements. Today, two main types of railway substructures are used worldwide: ballasted track systems and ballastless track systems. A ballasted track consists of a pair of rails, sleepers, and fastening systems supported by a ballast layer. Its main advantage lies in its low construction cost and effective drainage performance, although regular maintenance is always required [1]. In contrast, ballastless tracks feature a concrete roadbed in which the sleepers are embedded—commonly known as a slab track [2].

Mineralogically, ballast waste consists of silicates and kaolinitic clay minerals [3]. Most of this waste is either used as inert material or stored in waste dumps or landfills, presenting significant technical, economic, and environmental challenges.

With continued use, ballast becomes rounded and loses the properties that make it suitable for supporting the weight of the track structure, ultimately turning into inert waste that is sent to landfills. However, different studies have shown that this waste can

be repurposed, particularly as supplementary cementitious material (SCMs), replacing cement in different proportions for cement and concrete production. The incorporation of various types of waste into cement—such as fly ash, slag, sewage sludge, plant waste, and, more broadly, construction and demolition waste, including ballast waste—is a widely accepted practice.

Supplementary cementitious materials (SCMs) are multiphase heterogeneous materials whose properties are influenced by the characteristics of each component [4]. This necessitates the study of the microstructure of the construction element, which has been carried out in different works using mercury intrusion porosimetry (MIP), one of the most widely used techniques for determining pore size distribution, from capillary pores to air voids in cement paste samples [5]. X-ray diffraction (XRD) can be employed for qualitative and semiquantitative analysis of the components present in powdered samples [6]. Scanning electron microscopy (SEM) provides microstructural information on the sample surface through high-resolution imaging [7]. Additionally, nuclear magnetic resonance (NMR), a non-destructive technique, can be used to examine extremely fine components such as C-S-H gels and capillary pores [8,9]. The pore structure is one of the most critical characteristics of cement-based materials, directly affecting mechanical properties, transport properties, and durability.

The microstructure of these materials has been characterized through various properties, including permeability [10,11], thermal conductivity [12], strength [13], carbonation [14–16], freeze—thaw resistance [17], chloride attack resistance [18], porous structure [19–21], pore connectivity [22], hydration [23–25], damage evolution [26], and deterioration [27], along with physical properties such as mass diffusivity [28], among others.

Recently, X-ray micro-computed tomography (μ -CT) has contributed significantly to the study of porous structures in materials [29], as it does not require special sample preparation. This aspect is particularly important for studies involving Portland cement-based materials, where many conventional sample preparation procedures can alter the structure of the cement paste.

The role of additives in cement-based systems has been extensively studied, not only for sustainability and cost-effectiveness, but also due to the advantages these materials provide in the final cement product [30]. The cost and environmental impact of cement production are constrained by sustainability concerns, and also by the benefits associated with pozzolanic binders added to cement. In addition to these advantages, blended materials exhibit improved micro- and macrostructural properties [31]. When pozzolanic materials are incorporated into cement-based systems, they react with portlandite formed during cement hydration [32], modifying both fresh and hardened-state properties. Changes in particle size distribution influence setting times [33] and viscosity. At early hydration stages, pozzolanic materials act primarily as fillers, increasing the effective water-to-binder ratio and reducing hydration heat [34,35]. At later stages, they contribute pozzolanically, enhancing cement properties. These structural modifications improve macro-properties, such as expansion control [36] and durability [37].

The aim of this study is to analyze the behavior of novel silico-aluminous mineral additions with pozzolanic activity and added value in cement manufacturing and similar materials. Specifically, the study investigates the use of railway infrastructure waste—track ballast—as a replacement material in pozzolanic cement for applications in slab tracks and concrete sleepers. The research aims to evaluate the pore structure (porosity and other morphological parameters) of a cement matrix composite using μ -CT on an intact sample. Initially, the pozzolanic characteristics of the materials and their workability in their raw state will be examined.

2. Materials and Methods

2.1. Materials

Two types of rock samples, used as ballast in track renewal works near the extraction site, were selected for this study. To simulate ballast residue, rock fragments were subjected to the Los Angeles abrasion test [38], which assesses the suitability of ballast for its intended use under the conditions specified in Annex C of the standard [39]. The abraded material was collected for use in the tests conducted in this study.

- Sample B-1: Hornfels with a granoblastic texture, matte luster, and opaque colors. The extraction area is located in Aldeavieja, Ávila (Spain) [40] (Figure 1).
- Sample B-2: Dark-colored porphyritic rock. The sampling area is located on cartographic sheet No. 531 of the Geological Map of Spain (scale 1:50,000), "Ávila de los Caballeros" (Ávila, Spain) [41] (Figure 2).

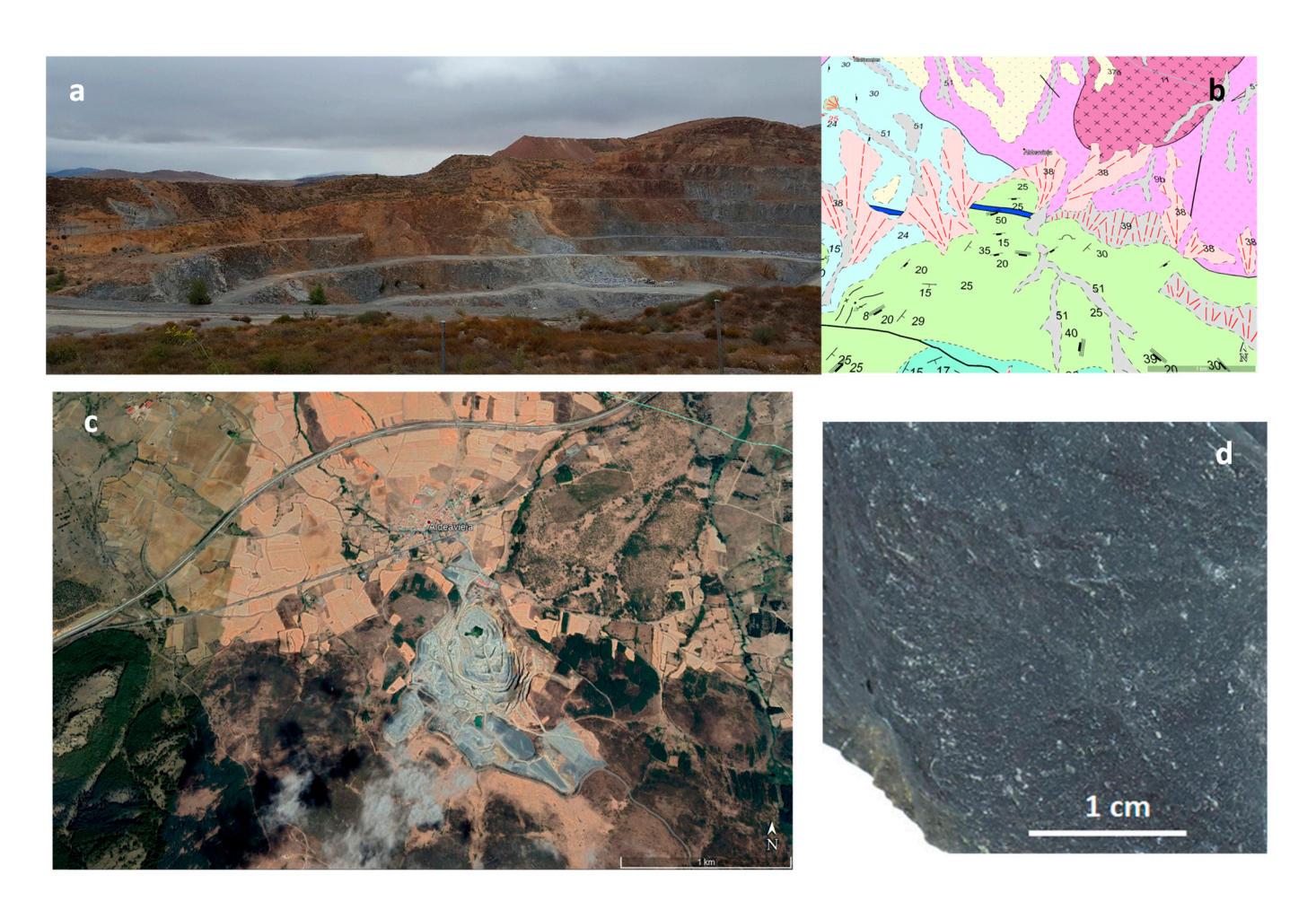


Figure 1. Sample B-1. (a) General view of the quarry. (b) Geological map of the area. (c) Aerial photograph. (d) Hand-shown material. Source: Google Earth Pro. Scale: 1:1000.

Mortar specimens were prepared using ordinary Portland cement (CEM I 42.5N) and mixtures of the same cement with 10%, 15%, and 20% replacement of the selected waste material. The specimens were produced in accordance with relevant standards [42–45], with dimensions of 4 cm \times 4 cm \times 16 cm for testing. When preparing mortars with replacement materials, grain size is a crucial factor. According to [46], replacement levels around 10% can improve mechanical and elastic properties when different particle sizes are combined, preventing homogeneity.

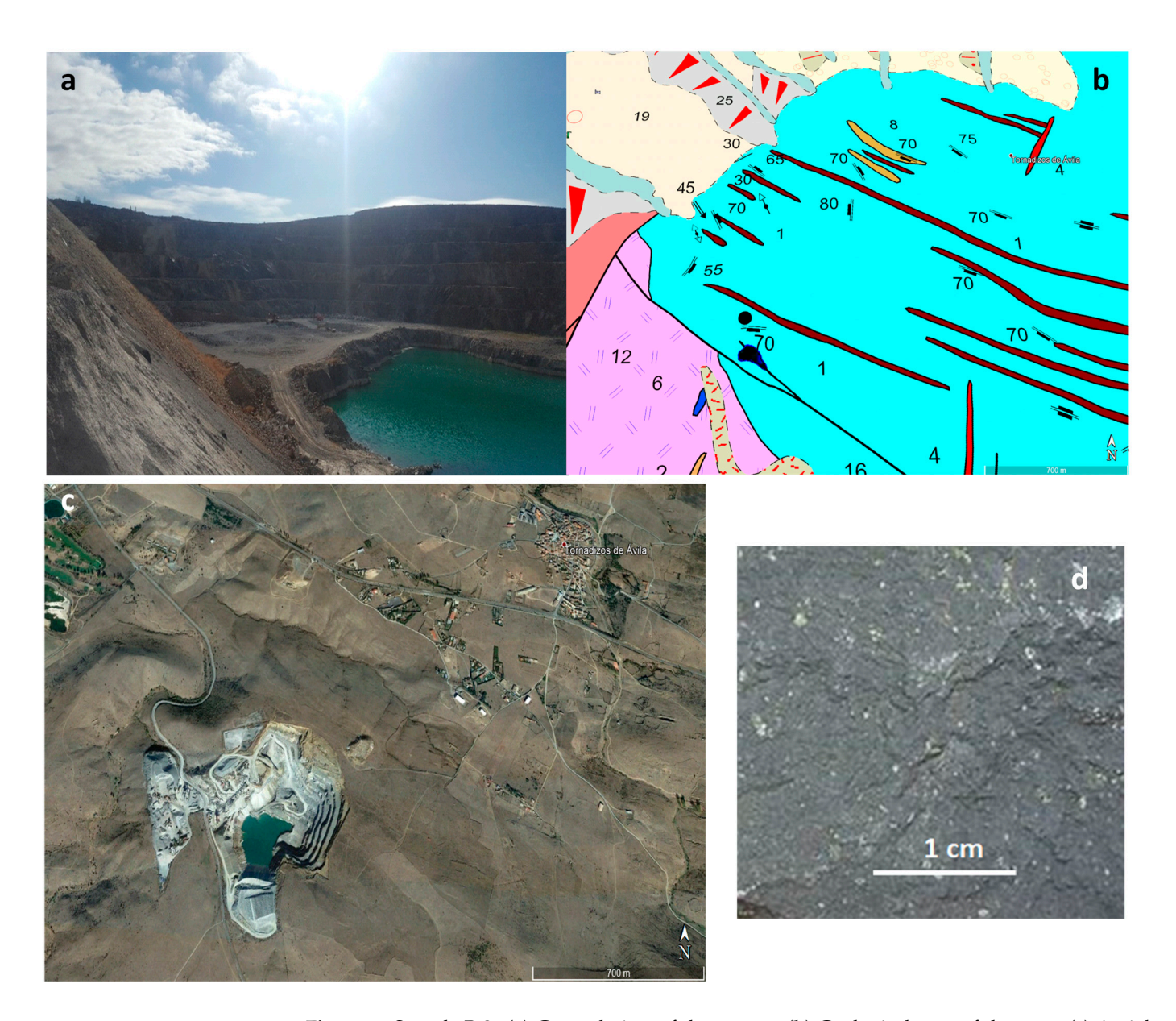


Figure 2. Sample B-2. (a) General view of the quarry. (b) Geological map of the area. (c) Aerial photograph. (d) Hand-shown material. Source: Google Earth Pro. Scale: 1:700.

The ordinary Portland cement (OPC) used in this study is CEM I 42.5 R, supplied by the Lafarge Holcim cement plant in Villaluenga de la Sagra (Toledo, Spain). The sand used is a UNE-EN 196-1 standardized natural sand [47], with a silica content of \geq 98%.

2.2. Methods

The particle size distribution was determined using laser diffraction spectrometry (LDS), within a measurement range of 0.1 μm to 1750 μm . The analysis was performed with a Sympatec Helos 12 LA spectrometer (Sympatec, Clausthal-Zellerfeld, Germany) in a wet system, where the samples were subjected to shaking and ultrasound treatment to maximize particle dispersion in a non-reactive liquid—in this case, isopropyl alcohol.

The solid phase identification was carried out by X-ray diffraction (XRD) using a SIEMENS D-5000 X-ray diffractometer (Siemens, Madrid, Spain). The unoriented powder diffractogram was recorded within a 5° to 60° range, at a scan rate of 2° per minute. The X-ray generator tube used a tungsten filament with a copper anode (Cu K α radiation). The applied current and voltage were 30 mA and 40 kV, respectively, while the divergence and

receiving slits measured 1° and 0.18° , respectively. Phase identification and quantification were performed using Match! v.3 and Rietveld FullProf software (version 8.20), with data from the Inorganic Crystal Structure Database (ICSD) and the Crystallography Open Database (COD), using rutile as an internal standard.

For SEM/EDX analysis, a PHILIPS XL scanning electron microscope (Philips, Eindhoven, The Netherlands) with a tungsten source was used. Samples were fixed onto a metallic sample holder with double-sided graphite adhesive tape and, subsequently, gold-coated using a BIO-RAD SC 502 sputter coater (Bio-Rad Laboratories, Inc., Hercules, CA, USA) to ensure conductivity. The same electron microscopy system was used for point chemical analysis, employing energy-dispersive X-ray spectroscopy (EDX) with a silicon/lithium detector and a DX4i EDX analyzer (IXRF Systems, Hillsboro, OR, USA).

Since the mechanical strength of cement-based materials is closely related to the microporosity of the cementitious matrix, this characteristic was assessed using X-ray computed tomography (CT). A NIKON XT-H-160 CT scanner (Nikon, Leuven, Belgium) was used, equipped with a W-target, a 0.375 mm Cu filter, and a 708 ms exposure time per frame, capturing a total of four frames with 1100 to 155 kV and 57 μ A settings. This setup allowed for cross-sectional imaging of the internal structures.

To evaluate pozzolanic activity, an accelerated method was applied. In total, 1 g of the sample was placed in 75 mL of a saturated calcium hydroxide solution (17.68 mM/L) at $40\,^{\circ}$ C for 1, 7, 14, 28, and 90 days. At each time interval, the solution was vacuum-filtered through a Büchner funnel, and the calcium ion concentration, expressed as calcium oxide (fixed lime), was determined following the procedure detailed in the standard [48].

The chemical characterization was performed using inductively coupled plasma mass spectrometry (ICP-MS) with a PerkinElmer Elan 6000 spectrometer (Perkin Elmer, Wellesley, MA, USA), equipped with an AS91 automatic injector.

3. Results and Discussion

3.1. Initial Samples

3.1.1. Mineralogical Composition

Sample B-1. The mineralogical analysis is presented in Table 1. The composition is dominated by silicates, which are the most abundant minerals. Notable phases include biotite, quartz, kaolinite, and hematite. In terms of feldspars, the sample contains orthoclase (potassium aluminosilicate) and albite (sodium aluminosilicate), along with a fraction of amorphous material.

Table 1. Rietveld quantification of the studied samples (RB and X^2 = agreement factors; n.d. = not detected).

Ballast Waste	R_B	X ²	Biotite (%)	Kaolinite (%)	Quartz (%)	Orthoclase (%)	Albite (%)	Amorphous Material (%)	Hematite (%)	Labradorite (%)
B-1	16.5	3.3	30	7	29	6	14	10	4	n.d.
B-2	12.3	3.5	35	6	21	5	n.d.	6	4	23

Sample B-2: Its mineralogical composition is similar to that of Sample B-1, but with lower quartz content. Additionally, albite is absent, being replaced by labradorite (calcium aluminosilicate) (Table 1).

The ballast residues, rich in silicates (quartz, feldspars, phyllosilicates), contribute to ordinary Portland cement (OPC) (which is rich in alkalis) by introducing a siliconand aluminum-dominated composition. This enhances cement properties, particularly workability, leading to the production of ecological pozzolanic cement. This process

promotes sustainability by incorporating waste and recycled materials into the cement manufacturing cycle, replacing naturally extracted resources, some of which are becoming scarce. The grinding and fineness of the material disrupt crystalline structures, increasing specific surface area and thereby facilitating the pozzolanic reaction [49].

3.1.2. Chemical Composition

The major element analysis indicates that the combined content of silicon, aluminum, and iron oxides exceeds 85%. Additionally, Sample B-2 exhibits higher sodium and calcium concentrations, which is attributed to the presence of labradorite (Table 2). Its loss on ignition (LOI) is slightly higher than that of Sample B-1. Regarding the minor and trace element analysis, both samples contain Li, Be, Sc, V, Cr, Co, Ni, Cu, Zn, Ga, Ge, As, Se, Rb, Sr, Y, Zr, Nb, Sn, Cs, La, Ce, Pr, Nd, Sm, Gd, Dy, Er, Yb, Hf, Ta, W, Tl, Pb, Bi, and U.

Oxides (%)	B-1 Sample	B-2 Sample
Na ₂ O	2.97	4.78
MgO	1.72	0.95
Al_2O_3	13.79	19.60
K ₂ O	2.85	4.06
CaO	2.77	3.26
MnO	0.11	0.03
TiO_2	0.80	0.37
Fe_2O_3	6.72	3.49
SiO_2	68.27	63.49
LOI	0.67	1.22

Table 2. Chemical analysis of the major elements (LOI = loss in ignition).

All this leads us to believe that this acidic composition, along with a small particle size, will exhibit significant pozzolanic activity.

3.1.3. Pozzolanicity

For both samples, B-1 and B-2, the pozzolanic activity was assessed to determine the activation capacity of this ballast waste. The accelerated method was used over 1, 7, 14, 28, 90, 180, and 360 days, measuring the calcium concentration—expressed as calcium oxide or fixed lime—according to the standard [48].

The pozzolanicity test results for both study samples are presented in Figure 3. The fixed lime measurements are very similar, with slightly lower values in sample B-1 at early ages (indicating a slightly slower lime fixation). However, after more than 90 days of pozzolanic reaction, the trend reverses. When comparing this type of addition—ballast waste—with other materials used in the cement industry, such as silica fume, fly ash, or even non-standardized additions like sanitary ceramic waste or slag from the steel or copper industry [50] a similar behavior was initially seen, with slow pozzolanic activity. However, by 28 days—the age considered in the regulations—a greater lime fixation capacity was achieved compared with those reported in the literature.

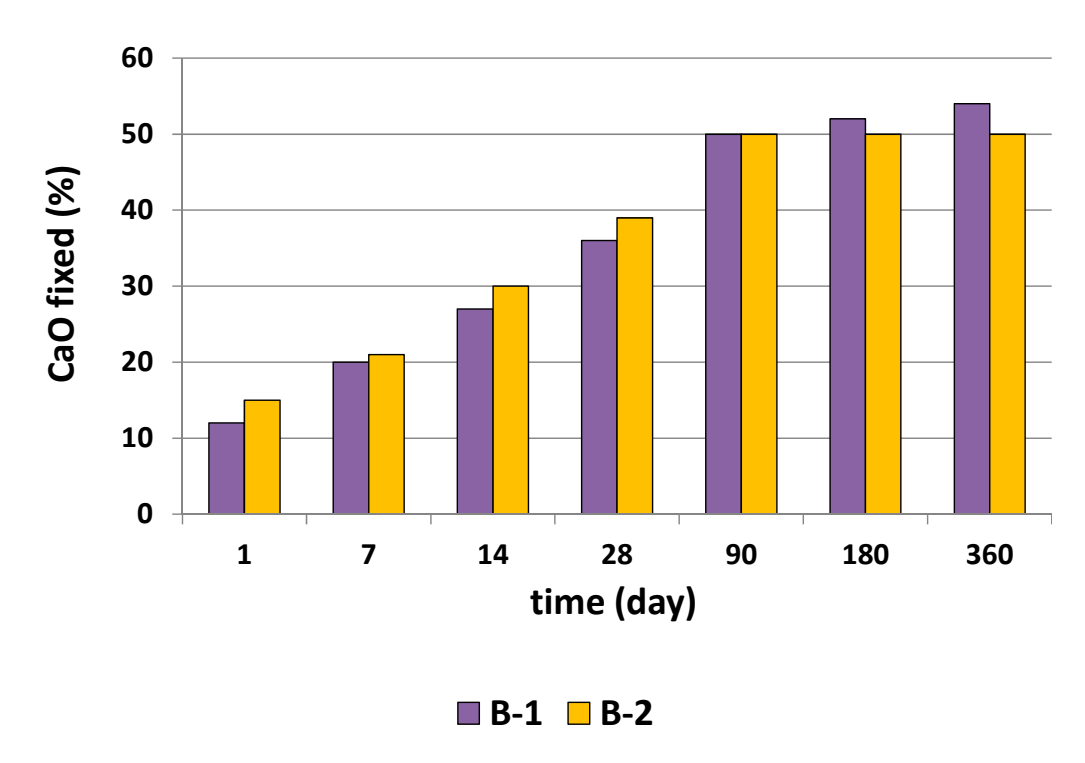


Figure 3. Variation in pozzolanic activity with reaction time in the samples studied.

3.1.4. Particle Size

The particle size distribution curves for both samples are similar, exhibiting two peaks: one around 6 μm for both, and a second at 9.5 μm for sample B-2 and 15 μm for sample B-1 (Figure 4). These results suggest that, based on particle size, both samples can be considered potential pozzolans.

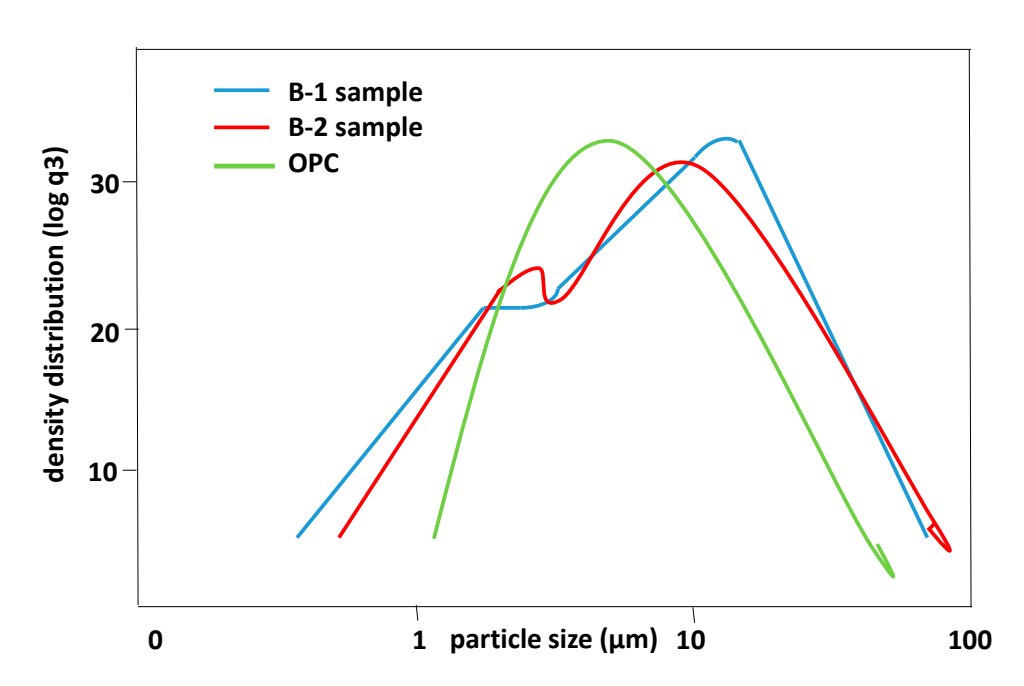


Figure 4. Particle size distribution density curves in all samples studied.

3.2. Preparation of Mortars with Ballast Waste

For the preparation of mortars with ballast waste, standardized CEN sand with a particle size between 1 mm and 0.08 mm was used, meeting the specified requirements [47]. The cement used was an early-age reactive cement [51], primarily composed of CaO, and

followed by silica, with smaller amounts of alumina, iron oxides, magnesium oxides, and alkaline elements. The mixture of ballast waste and Portland cement ensured material homogeneity. Replacements of 10%, 15%, and 20% ballast waste by weight were prepared in the OPC. Workability was evaluated in the fresh state, while porosity was analyzed in the hardened state.

3.2.1. Workability

In cement-based materials, the fresh state corresponds to the time between cement hydration and setting, during which the material exhibits plastic behavior. Workability tests were conducted on cements with 10%, 15%, and 20% ballast waste replacement (sample B-1 and sample B-2). The selected water/cement ratio for the test was 0.5, and the cement replacement/sand ratio was 1:3.

Before mixing, the reference cement (OPC) and the ballast replacement dosages were blended in a tubular device for five minutes to prevent segregation during mixing, which was carried out using Controls-brand equipment [47].

The mortar consistency results are shown in Figure 5. For each type of cement, average values from three consistency determinations are provided. Additionally, the loss of fluidity in the cement with ballast replacement, relative to OPC, is represented and calculated using Equation (1).

$$Loss\ of\ fluidity = \frac{(medium\ consistency\ reference-mediaum\ consistency\ cement)}{mediaum\ consistency\ reference} \times 100 \tag{1}$$

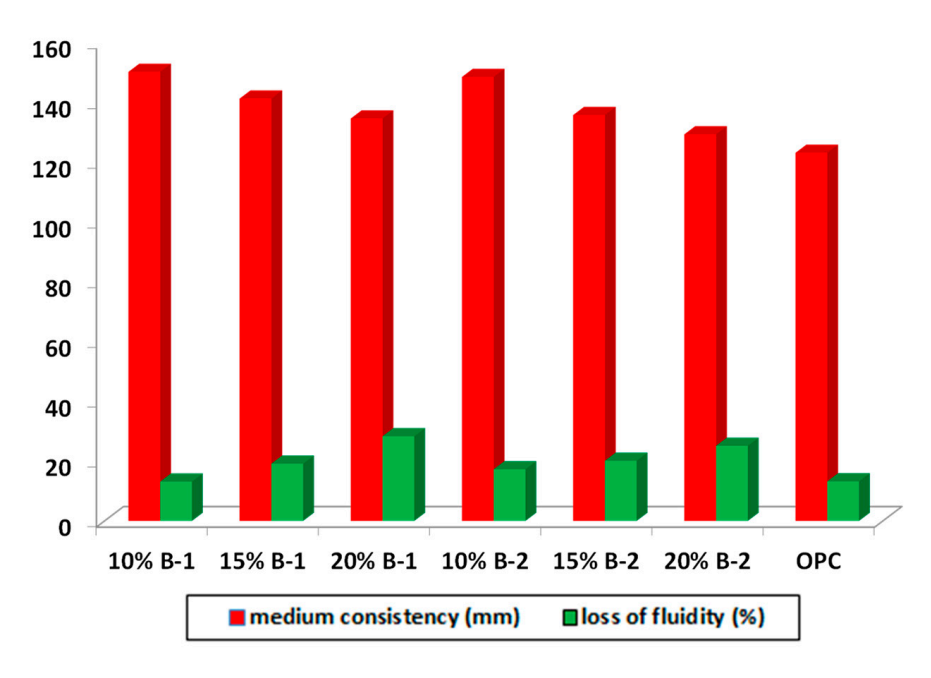


Figure 5. Representation of the values of fluidity loss and average consistency in all mortars.

In general, a decrease in the spread diameter (mean consistency) is observed as the replacement percentage increases from 10% to 20%. The loss of fluidity in the cement with the replacement follows a linear trend as the ballast waste replacement percentage increases (from 10% to 20%) (Figure 5).

The mean consistency of both samples studied is similar, and decreases as the replacement percentage increases. The results are also similar for fluidity loss, which increases with the ballast waste replacement percentage in OPC.

Studies on cement with replacement using siliceous materials [52–55] show that the resulting mixtures require a higher water demand to maintain workability. The replacement

of small amounts of cement (5% by mass) with kaolin has little effect on paste fluidity. However, at higher replacement percentages (above 10%), the addition of water-reducing agents or superplasticizers is usually necessary to ensure workability.

Regarding workability, the pozzolanic activity of cements with the studied sample substitutions has been determined using the Frattini test, with testing times of 8 and 15 days, according to the standard. The values obtained have been presented in Figure 6.

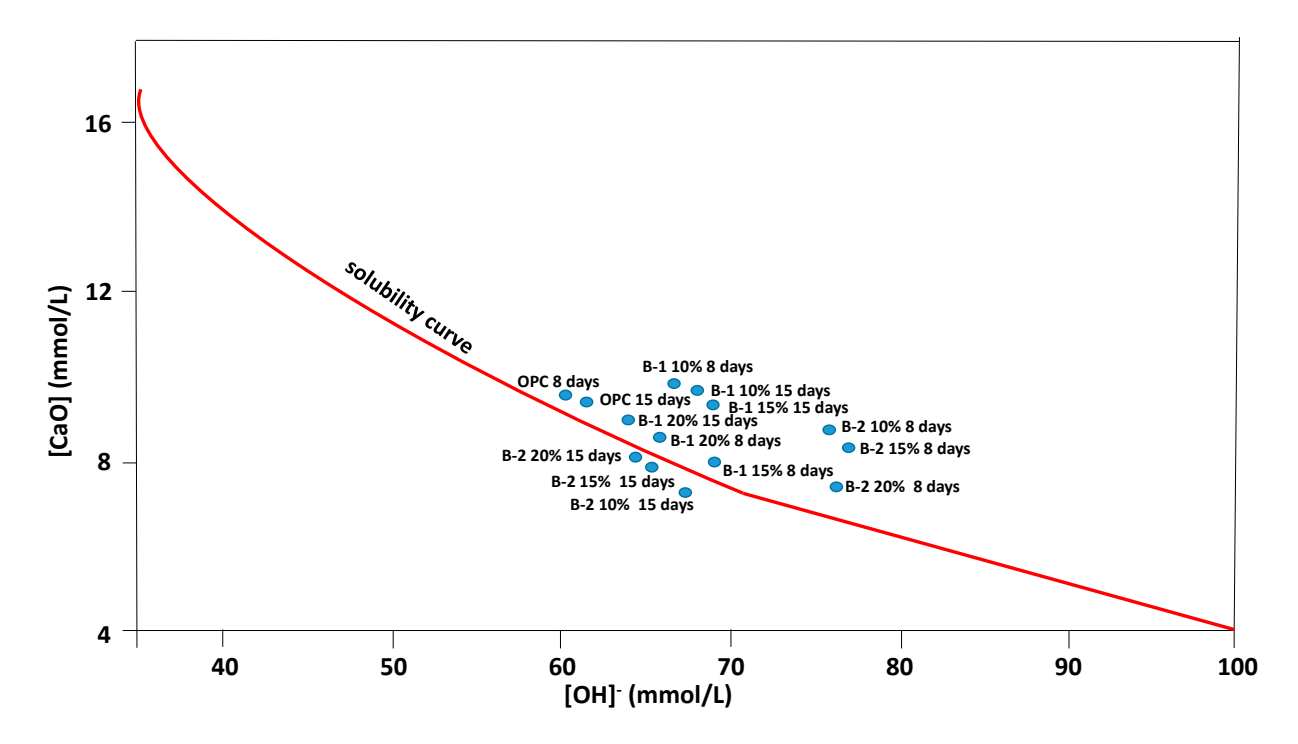


Figure 6. Frattini diagram with values obtained from the studied samples.

All samples with substitutions at 8 days are located above the CaO solubility curve, with a tendency to be positioned to the left of the CaO/OH⁻ solubility curve relative to OPC. This corresponds to an increase in the concentration of Ca²⁺ released during the hydration process of the new cements. The sample B-2 mortars at 8 days deviate from the rest and from OPC, although they maintain the tendency to be positioned above the solubility curve.

Meanwhile, the sample B-2 mortars with the three substitutions at 15 days are below the CaO solubility limit curve, due to a lower calcium ion content released during the hydration reaction. This condition allows these cements to be classified as Class IV pozzolanic-type cements [56].

The situation appears to coincide with the pozzolanic activity data, that is, with the low activity at an early age up to 28 days, attributed to a filler effect during this period [57], causing a nucleation process in which more space is available for the precipitation of hydration products. In contrast, at ages beyond 28 days, the filler effect is replaced by the pozzolanic effect, leading to a decrease in portlandite content and the release of calcium ions.

3.2.2. Porosity

Over time, cement-based materials set, harden, and acquire the properties of a solid material. Various tests must be conducted to assess their stability. One of the key properties is porosity. The porous structure of mortars refers to the system formed by all the pores contained within them and their distribution throughout the material. The response to different aggressive actions (physical, chemical, and biological) from the environment is influenced by the transport of substances within this porous structure.

Among the different types of porosity, the type related to interconnected pores is particularly important, as it represents the maximum reversible water content. This porosity is directly associated with the transport of liquids and gases, the exchange of dissolved substances, and the tortuosity of the pathways [58].

Depending on pore size, they can be classified as macropores, mesopores or capillary pores, and micropores. The first category corresponds to air bubbles naturally trapped (compaction pores) and/or those intentionally included (entrained air pores). The second category includes pores located outside the cement gel compounds; these pores have variable shapes and may or may not be interconnected and open to the exterior. The last category consists of pores within the hydrated and hardened paste, which generally do not exchange fluids with the surrounding environment.

The pore types most directly related to durability and substance transport are macropores and capillary pores. A quantification of macropores in the samples yielded the results shown in Figure 7, highlighting the high number of small pores in the 20% substitution at the beginning of the material's hydration reaction. After one year, these pores had reduced to less than half. This is associated with the particle size of the ballast residue, which is smaller than that of OPC. Larger pores are most abundant in the 10% substitution after one year of reaction.

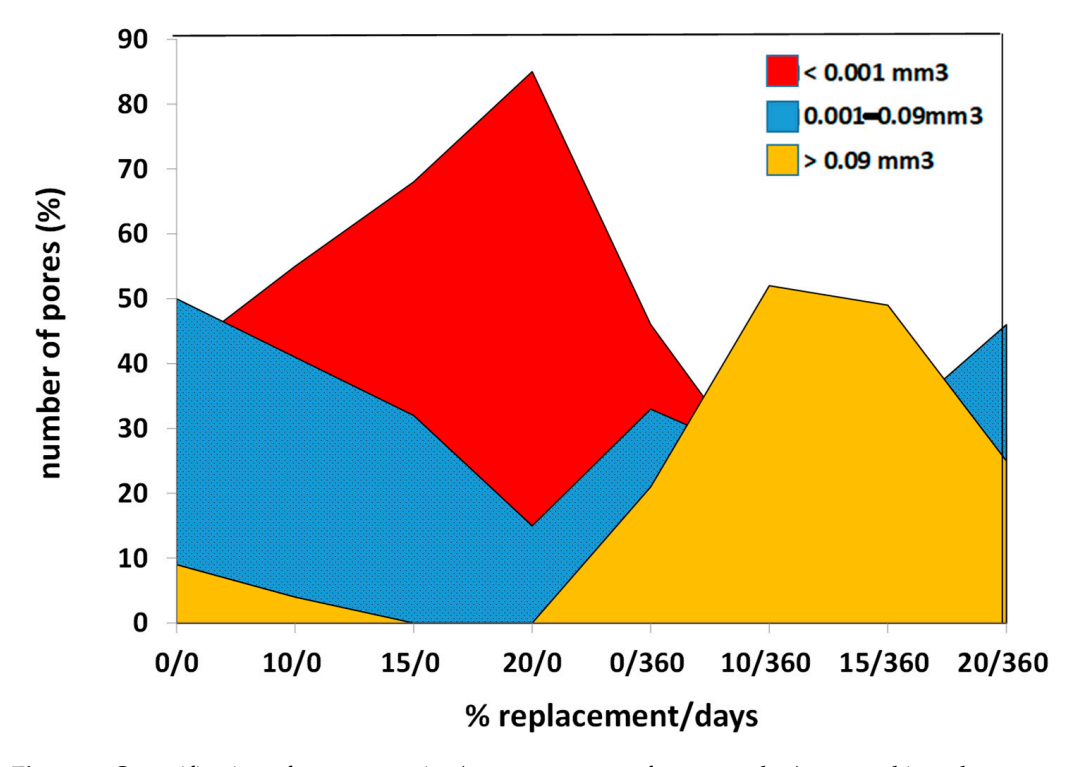


Figure 7. Quantification of macroporosity (as a percentage of pore number) grouped into three pore volume intervals ($>0.09 \text{ mm}^3$, $<0.09 \text{ mm}^3$, $<0.001 \text{ mm}^3$, and $<0.001 \text{ mm}^3$).

Large-volume pores are scarce at all reaction times and residue substitution proportions. Medium-volume pores in OPC remain constant throughout the entire hydration reaction. Small-volume pores are the most numerous, increasing in number throughout the test for both substitutions (Figure 8).

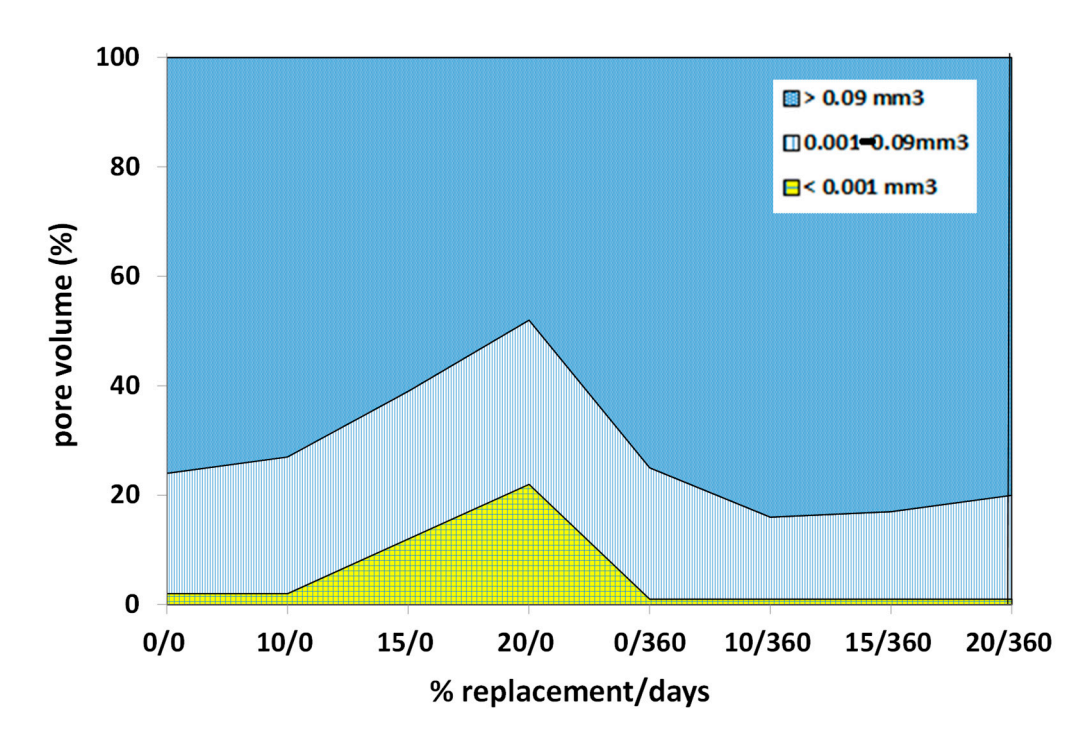


Figure 8. Quantification of macroporosity (as a percentage of pore volume) grouped into three pore volume intervals ($>0.09 \text{ mm}^3$, $<0.09 \text{ mm}^3$, and $<0.001 \text{ mm}^3$).

The total porosity values and the average pore size in mortars with residue substitution changed after one year compared to OPC, with a decrease in average pore size [13]. Regarding pore volume, the largest pores were the most abundant throughout the entire period considered. Intermediate pores were almost non-existent (Figure 9). Porosity is linked to the formation of C-S-H gels, whose morphology varies depending on the degree of hydration [59–62].

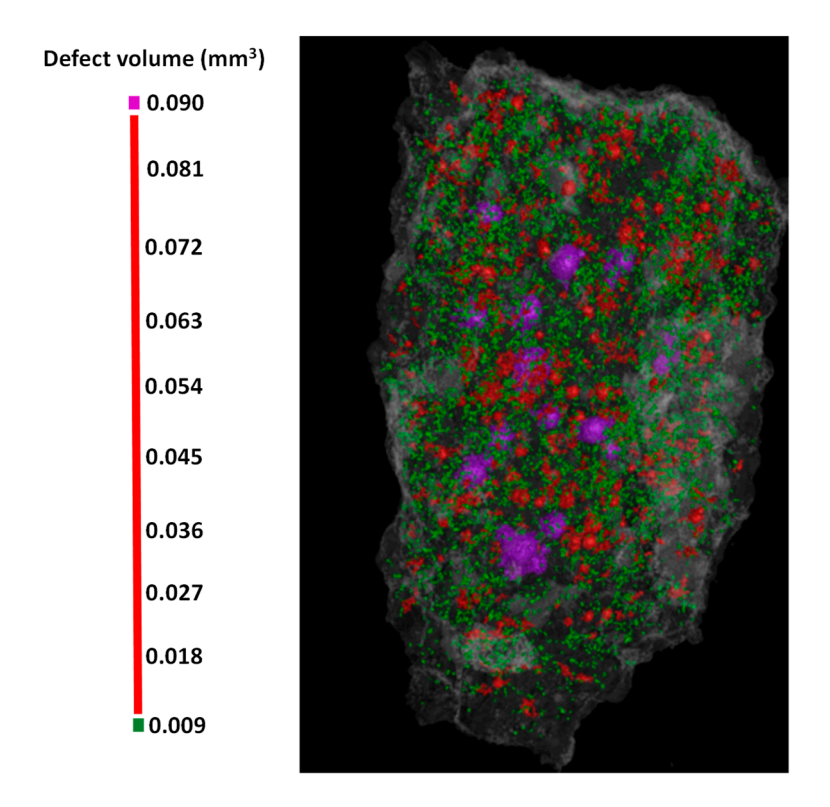


Figure 9. Representation of volume defects in the studied samples.

Small pores, which are predominant in mortars with a substitution, decrease in quantity over time, in contrast to larger-volume pores. SEM/EDX observations indicate that when the cement has no substitution, the contact between grains is formed by C-S-H gels and ettringite fibers, giving it a slightly porous appearance (Figure 10A,C). In contrast, when observing cement with a substitution, less-porous materials are generated (Figure 10B).

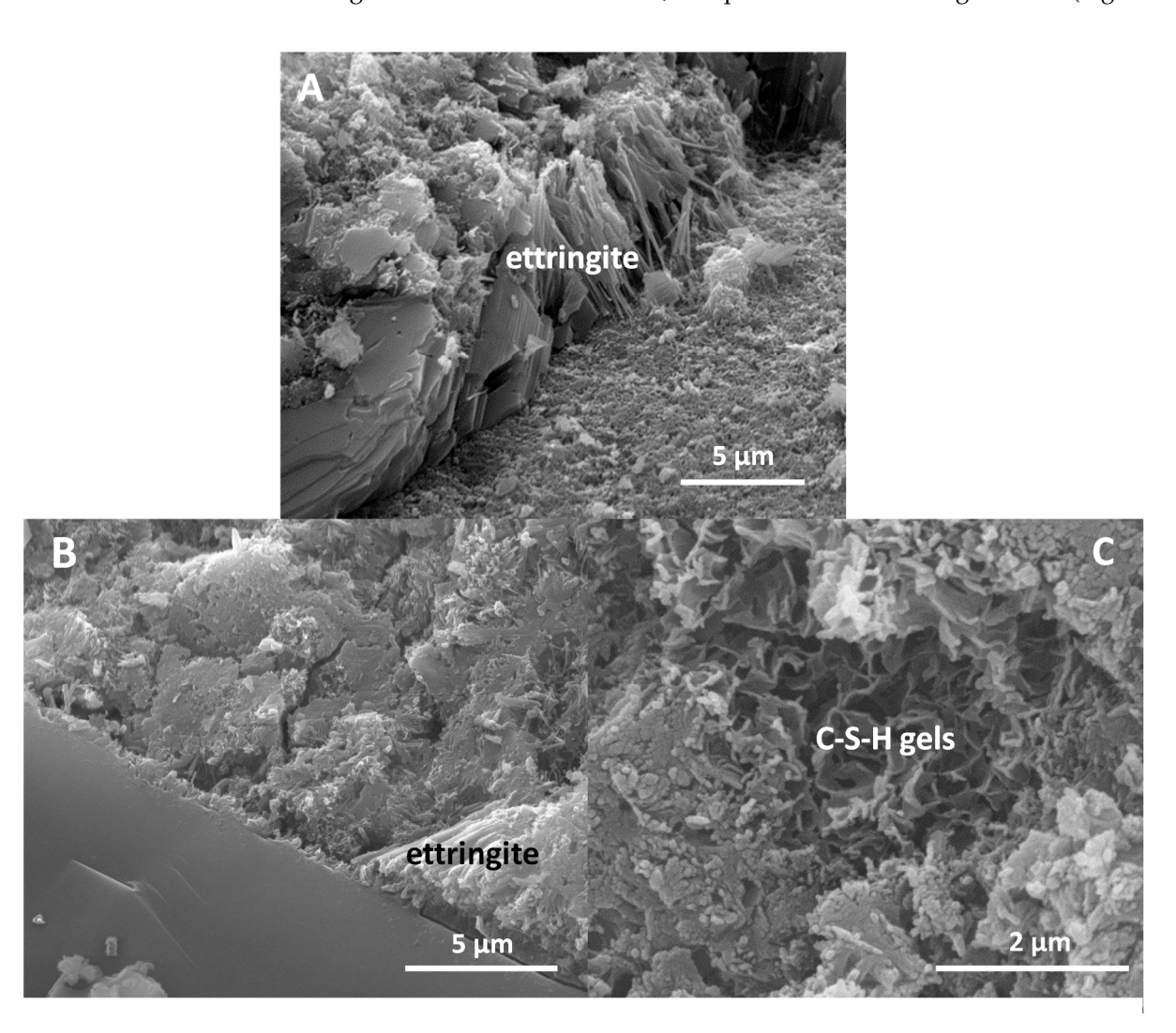


Figure 10. (A,C) Cement without substitution. (B) Cement with 15% substitution.

3.2.3. Pore Connectivity and Tortuosity

In relation to porosity, studies have been conducted on tortuosity, which is defined as the ratio between the length of the continuous path between two points and the shortest straight-line distance [63], and it can be calculated as proposed by Salmas and Androut-sopoulos [64].

Higher tortuosity in cement-based mixtures could be attributed to the greater refinement of pores and a faster hydration rate [65]. Conversely, moisture and ion transport are facilitated [66], which is not observed in the studied samples (Figure 9).

Over time, pores are filled by the precipitation of ettringite, interacting with C-S-H gels, as observed in Figure 10C.

4. Conclusions

Siliceous waste samples from railway ballast have been used as OPC substitutions to avoid landfill disposal and to utilize the waste as an SMC.

Pozzolanicity tests have been carried out with natural samples. After one year of reaction and monitoring at 1, 7, 28, 90, 180, and 360 days, all samples presented pozzolanic activity, with the highest values observed for sample B-1, which contains a high amount of amorphous material.

When a 10% ballast waste substitution is prepared, the same compounds are produced as in cement without a substitution, coexisting with the raw waste minerals (quartz, feldspar, mica, kaolinite, and hematite). With a 20% substitution, the hydration processes are similar to those observed for the 10% substitution in terms of the obtained hydration products and those inherited from the initial composition. A significant amount of C-S-H gels and LDH compounds form, but the behavior of portlandite differs. Portlandite decreases at medium reaction times and remains at longer times.

The shortest setting times correspond to waste substitutions with the highest percentage; this is related to particle size and the presence of amorphous material, thereby reducing setting time.

The workability of mortars with a substitution indicates that the average consistency decreases as the substitution percentage increases, while the loss of fluidity grows with a higher substitution percentage.

The total porosity and average pore size in mortars with a substitution are modified compared to OPC: there is a decrease in the 0.001 to 0.09 mm³ porosity in mortars with 10% and 20% substitutions. The most abundant pore volume is greater than 0.09 mm³, maintaining a constant number throughout the hydration reaction. Intermediate pores are fewer in number with the 10% substitution, while in the 20% substitution, the largest pores are almost non-existent.

Porosity is linked to the formation of C-S-H gels and the presence of ettringite, which fills the pores between particles. Tortuosity can be considered low, which hinders the transport of aqueous solutions, making the substituted cements studied more resistant to hydration processes.

Author Contributions: S.Y.-G. carried out the interpretation of the data and the writing of the paper. R.G.-G. analyzed the samples and interpreted the results. All authors have read and agreed to the published version of the manuscript.

Funding: This research received no external funding.

Institutional Review Board Statement: Not applicable.

Informed Consent Statement: Not applicable.

Data Availability Statement: The original contributions presented in this study are included in the article. Further inquiries can be directed to the corresponding author.

Conflicts of Interest: The authors declare no conflicts of interest.

References

- Nimbalkar, S.; Indraratna, B.; Dash, S.K.; Christie, D. Improved Performance of Railway Ballast under Impact Loads Using Shock Mats. J. Geotech. Geoenviron. Eng. 2012, 138, 281–294. [CrossRef]
- 2. Sheng, X.W.; Zheng, W.Q.; Zhu, Z.H.; Qin, Y.P.; Guo, J.G. Full-scale fatigue test of unit-plate ballastless track lay on long-span cable-stayed bridge. *Constr. Build. Mater.* **2020**, 247, 118601. [CrossRef]
- 3. Yagüe García, S.; Gonzalez Gaya, C. Durability analysis of pozzolanic cements containing recycled track ballast: Sustainability under extreme environmental conditions. *Constr. Build. Mater.* **2020**, 242, 117999. [CrossRef]
- 4. Neville, A.M. *Properties of Concrete*; Wiley: Chichester, UK, 2012.
- 5. Kumar, R.; Bhattacharjee, B. Study on some factors affecting the results in the use of MIP method in concrete research. *Cem. Concr. Res.* **2003**, *33*, 417–424. [CrossRef]
- 6. Elinwa, A.U.; Umar, M. X-ray diffraction and microstructure studies of gum arabic-cement concrete. *Constr. Build. Mater.* **2017**, 156, 632–638. [CrossRef]

7. Wang, X.S.; Wu, B.S.; Wang, Q.Y. Online SEM investigation of microcrack characteristics of concretes at various temperatures. *Cem. Concr. Res.* **2005**, *35*, 1385–1390. [CrossRef]

- 8. Wyrzykowski, M.; McDonald, P.J.; Scrivener, K.L.; Lura, P. Water redistribution within the microstructure of cementitious materials due to temperature changes studied with ¹H NMR. *J. Phys. Chem. C* **2017**, *121*, 27950–27962. [CrossRef]
- 9. Zhang, J.; Bian, F.; Zhang, Y.; Fang, Z.; Fu, C.; Guo, J. Effect of pore structures on gas permeability and chloride diffusivity of concrete. *Constr. Build. Mater.* **2018**, *163*, 402–413. [CrossRef]
- 10. Chung, S.Y.; Han, T.S.; Kim, S.Y. Reconstruction and evaluation of the air permeability of a cement paste specimen with a void distribution gradient using CT images and numerical methods. *Constr. Build. Mater.* **2015**, *87*, 45–53. [CrossRef]
- 11. Sokhansefat, G.; Ley, M.T.; Cook, M.D.; Alturki, R.; Moradian, M. Investigation of concrete workability through characterization of aggregate gradation in hardened concrete using X-ray computed tomography. *Cem. Concr. Compos.* **2019**, *98*, 150–161. [CrossRef]
- 12. Chung, S.Y.; Elrahman, M.A.; Stephan, D. Investigation of the effects of anisotropic pores on material properties of insulating concrete using computed tomography and probabilistic methods. *Energy Build.* **2016**, 125, 122–129. [CrossRef]
- 13. Zhang, H.; Šavija, B.; Lukovic, M.; Schlangen, E. Experimentally informed micromechanical modelling of cement paste: An approach coupling X-ray computed tomography and statistical nanoindentation. *Compos. Part B Eng.* **2019**, *157*, 109–122. [CrossRef]
- 14. Han, J.; Liu, W.; Wang, S.; Du, D.; Xu, F.; Li, W.; de Schutter, G. Effects of crack and its and aggregate on carbonation penetration based on 3D micro x-ray CT microstructure evolution. *Constr. Build. Mater.* **2016**, *128*, 256–271. [CrossRef]
- 15. Liu, J.; Ba, M.; Du, Y.; He, Z.; Chen, J. Effects of chloride ions on carbonation rate of hardened cement paste by x-ray CT techniques. *Const. Build. Mater.* **2016**, 122, 619–627. [CrossRef]
- 16. Cui, D.; Banthia, N.; Wang, Q.; Sun, W. Investigation on porosity of partly carbonated paste specimens blended with fly ash through dual CT scans. *Constr. Build. Mater.* **2019**, 196, 692–702. [CrossRef]
- 17. Shields, Y.; Garboczi, E.; Weiss, J.; Farnam, Y. Freeze-thaw crack determination in cementitious materials using 3D X-ray computed tomography and acoustic emission. *Cem. Concr. Compos.* **2018**, *89*, 120–129. [CrossRef]
- 18. Qi, B.; Gao, J.; Chen, F.; Shen, D. Chloride penetration into recycled aggregate concrete subjected to wetting-drying cycles and flexural loading. *Constr. Build. Mater.* **2018**, 174, 130–137. [CrossRef]
- 19. Gallucci, E.; Scrivener, K.; Groso, A.; Stampanoni, M.; Margaritondo, G. 3D experimental investigation of the microstructure of cement pastes using synchrotron X-ray microtomography. *Cem. Concr. Res.* **2007**, *37*, 360–368. [CrossRef]
- 20. Bossa, N.; Chaurand, P.; Vicente, J.; Borschneck, D.; Levard, C.; Chariol, O.A.; Rose, J. Micro- and nano-X-ray computed-tomography: A step forward in the characterization of the pore-network of a leached cement paste. *Cem. Concr. Res.* **2015**, *67*, 138–147. [CrossRef]
- 21. du Plessis, A.; Olawuyi, B.; Boshoff, W.; le Roux, S. Simple and fast porosity analysis of concrete using X-ray computed tomography. *Mater. Struct.* **2016**, *49*, 553–562. [CrossRef]
- 22. Lu, S.; Landis, E.; Keane, D. X-ray microtomographic studies of pore structure and permeability in Portland cement concrete. *Mater. Struct.* **2006**, *36*, 11–20.
- 23. Chotard, T.; Boncoeur-Martel, M.; Smith, A.; Dupuy, J.; Gault, C. Application of X ray computed tomography to characterise the early hydration of calcium aluminate cement. *Cem. Concr. Compos.* **2003**, *25*, 145–152. [CrossRef]
- 24. Helfen, L.; Dehn, F.; Mikulik, P.; Baumbach, T. Three-dimensional imaging of cement microstructure evolution during hydration. *Adv. Cem. Res.* **2007**, *17*, 103–111. [CrossRef]
- 25. Gastaldi, D.; Canonico, F.; Capelli, L.; Boccaleri, E.; Milanesio, M.; Palin, L.; Croce, G.; Marone, F.; Mader, K.; Stampanoni, M. In situ tomographic investigation on the early hydration behaviors of cementing systems. *Constr. Build. Mater.* **2012**, 29, 284–290. [CrossRef]
- 26. Zhang, M.; Jivkov, A. Micromechanical modelling of deformation and fracture of hydrating cement paste using X-ray computed tomography characterisation. *Compos. Part B Eng.* **2016**, *88*, 64–72. [CrossRef]
- 27. Yang, Y.; Zhang, Y.; She, W.; Wu, Z.; Liu, Z.; Ding, Y. Nondestructive monitoring the deterioration process of cement paste exposed to sodium sulfate solution by X-ray computed tomography. *Constr. Build. Mater.* **2018**, *186*, 182–190. [CrossRef]
- 28. Zhang, M.; He, Y.; Lange, D.; Breggel, K. Computational investigation on mass diffusivity in Portland cement paste based on X-ray computed microtomography image. *Constr. Build. Mater.* **2012**, 27, 472–481. [CrossRef]
- 29. Ghiasvand, E.; Ramezanianpour, A.A.; Ramezanianpour, A.M. Effect of grinding method and particle size distribution on the properties of Portland-pozzolan cement. *Constr. Build. Mater.* **2014**, *53*, 547–554. [CrossRef]
- 30. Mehta, P.K. Studies on blended Portland cements containing santorin earth. Cem. Concr. Res. 1981, 11, 507–518. [CrossRef]
- 31. Taylor, H.F.W. Cement Chemistry; Thomas Telford: London, UK, 1997.
- 32. Lea, F.M. The Chemistry of Cement and Concrete; First Amer: New York, NY, USA, 1971.
- 33. John, E.; Lothenbach, B. Cement hydration mechanisms through time-a review. J. Mater. Sci. 2023, 58, 9805–9833. [CrossRef]
- 34. Deschner, F.; Winnefeld, F.; Lothenbach, B.; Seufert, S.; Schwesig, P.; Dittrich, S.; Goetz Neunhoeffer, F.; Neubauer, J. Hydration of Portland cement with high replacement by siliceous fly ash. *Cem. Concr. Res.* **2012**, *42*, 1389–1400. [CrossRef]

35. Ardoğa, M.K.; Erdoğan, S.T.; Tokyay, M. Effect of particle size on early heat evolution of interground natural pozzolan blended cements. *Constr. Build. Mater.* **2019**, 206, 210–218. [CrossRef]

- 36. Hamada, H.M.; Abdulhaleem, K.N.; Majdi, A.; Al Jawahery, M.S.; Skariah Thomas, B.; Yousif, S.T. The durability of concrete produced from pozzolan materials as a partially 625 cement replacement: A comprehensive review. *Mat. Today Proc.* 2023. [CrossRef]
- 37. Uzal, B.; Turanli, L. Studies on blended cements containing a high volume of natural pozzolans. *Cem. Concr. Res.* **2003**, *33*, 1777–1781. [CrossRef]
- 38. *UNE-EN 1097-2*; Ensayos para Determinar las Propiedades Mecánicas y Físicas de los Áridos; Parte 2: Métodos para la Determinación de la Resistencia a la Fragmentación. Asociación Española de Normalización y Certificación: Madrid, Spain, 2010.
- 39. UNE-EN 13450; Áridos para Balasto. Asociación Española de Normalización y Certificación: Madrid, Spain, 2003.
- 40. Martín Serrano, A.; del Olmo Sanz, A.; Bellido Mulas, F.; Fuster, J.; Navidad, M.; de Pablo Macía, J.; Villaseca, C. *Hoja* 1:50.000, *el Espinar*; Serie Magna; IGME: Madrid, Spain, 1991.
- 41. Martín Parra, L.; Martínez Salanova, I.; Moreno, F. Hoja 1:50.000, Ávila de los Caballeros; Serie Magna; IGME: Madrid, Spain, 2008.
- 42. ISO/TC 74; Cement and Lime. International Organization for Standardization: Geneva, Switzerland, 2009.
- 43. C150-07; Standard Specification for Portland Cement. ASTM International: West Conshohocken, PA, USA, 2007.
- 44. *ASTM C666-97*; Standard Test Method for Resistance of Concrete to Rapid Freezing and Thawing. ASTM International: West Conshohocken, PA, USA, 2017.
- 45. ASTM C469; Standard Test Method for Static Modulus of Elasticity and Poisson's Ratio of Concrete in Compression. ASTM International: West Conshohocken, PA, USA, 2010.
- Ostrowski, K.; Stefaniuk, D.; Sadowski, L.; Krzywinski, K.; Rozanska, M. Potential use of granite waste sourced from rock processing for the application as coarse aggregate in high-performance self-compacting concrete. *Constr. Build. Mat.* 2020, 238, 117–794. [CrossRef]
- 47. *UNE-EN 196-1*; Métodos de Ensayo de Cementos. Parte I. Determinación de Resistencias Mecánicas. Asociación Española de Normalización y Certificación: Madrid, Spain, 2018.
- 48. *UNE-EN 196-5*; Métodos de Ensayo de Cementos. Parte 5: Ensayo de Puzolanicidad para los Cementos Puzolánicos. Asociación Española de Normalización y Certificación: Madrid, Spain, 2011.
- 49. Souri, A.; Kazemi-Kamyab, H.; Snellings, R.; Naghizadeh, R.; Golestani-Fard, F.; Scrivener, K. Pozzolanic activity of mechanochemically and thermally activated kaolins in cement. *Cem. Concr. Res.* **2015**, 77, 47–59. [CrossRef]
- 50. Medina, G.; Sáez del Bosque, I.F.; Frías, M.; Sánchez de Rojas, M.I.; Medina, C. Mineralogical study of granite waste in a pozzolan/Ca(OH)₂ system. Influence of the activation process. *Appl. Clay Sci.* **2017**, *135*, 362–371. [CrossRef]
- 51. Richardson, I.G. The nature of the hydration products in hardened cement pastes. Cem. Concr. Comp. 2000, 22, 97–113. [CrossRef]
- 52. Sabir, B.B.; Wild, S.; Bai, J. Metakaolin and a calcined clays as pozzolans for concrete: A review. *Cem. Concr. Comp.* **2001**, 23, 441–454. [CrossRef]
- 53. Qian, X.; Li, Z. The relationships between stress and strain for high performance concrete with metakaolin. *Cem. Concr. Res.* **2001**, 31, 1607–1611. [CrossRef]
- 54. Sabir, B.B.; Wild, S.; Khabit, J.M. On the workability and strength development of metakaolin concrete. In Proceedings of the International Conference Concrete in the Service of Mankind, Dundee, UK, 24–28 June 1996; pp. 651–661.
- 55. Jones, T.R. Metakaolin as a Pozzolanic Addition to Concrete. In *Structure and Performance of Cements*, 2nd ed.; Bensted, J., Barnes, P., Eds.; Spon Press: London, UK, 2002; pp. 372–398.
- 56. *UNE-EN 197-1*; Cemento. Parte I: Composición, Especificaciones y Criterios de Conformidad de los Cementos Comunes. Asociación Española de Normalización y Certificación: Madrid, Spain, 2011.
- 57. Juenger, M.C.G.; Siddique, R. Recent advances in understanding the role of supplementary cementitious materials in concrete. *Cem. Concr. Res.* **2015**, *78*, 71–80. [CrossRef]
- 58. Shah, V.; Mackechnie, J.; Scott, A. Determination of carbonation resistance of concrete through a combination of cement content and tortuosity. *J. Build. Eng.* **2022**, *60*, 105176. [CrossRef]
- 59. Fonseca, P.C.; Jennings, H.M. The effect of drying on early-age morphology of C-S-H as observed in environmental SEM. *Cem. Concr. Res.* **2010**, *40*, 1673–1680. [CrossRef]
- 60. Bullard, J.W.; Jennings, H.M.; Livingston, R.A.; Nonat, A.; Scherer, G.W.; Schweitzer, J.S.; Scrivener, K.L.; Thomas, J.J. Mechanisms of cement hydration. *Cem. Concr. Res.* **2011**, *41*, 1208–1223. [CrossRef]
- 61. Gallucci, E.; Zhang, X.; Scrivener, K.L. Effect of temperature on the microstructure of calcium silicate hydrate (C-S-H). *Cem. Concr. Res.* **2013**, *53*, 185–195. [CrossRef]
- 62. Gartner, E.; Maruyama, I.; Chen, J. A new model for the C-S-H phase formed during the hydration of Portland cements. *Cem. Concr. Res.* **2017**, *97*, 95–106. [CrossRef]
- 63. Vervoort, R.W.; Cattle, S.R. Linking hydraulic conductivity and tortuosity parameters to pore space geometry and pore-size distribution. *J. Hydrol.* **2003**, 272, 36–49. [CrossRef]

64. Salmas, C.E.; Androutsopoulos, G.P. A novel pore structure tortuosity concept based on nitrogen sorption hysteresis data. *Ind. Eng. Chem. Res.* **2001**, *40*, 721–730. [CrossRef]

- 65. Bernardo, G.; Telesca, A.; Valenti, G.L. A porosimetric study of calcium sulfoaluminate cement pastes cured at early ages. *Cem. Concr. Res.* **2006**, *36*, 1042–1047. [CrossRef]
- 66. Mohan, M.K.; Rahul, A.V.; Van Stappen, J.F.; Cnudde, V.; De Schutter, G.; Van Tittelboom, K. Assessment of pore structure characteristics and tortuosity of 3D printed concrete using mercury intrusion porosimetry and X-ray tomography. *Cem. Concr. Comp.* 2023, 140, 105104. [CrossRef]

Disclaimer/Publisher's Note: The statements, opinions and data contained in all publications are solely those of the individual author(s) and contributor(s) and not of MDPI and/or the editor(s). MDPI and/or the editor(s) disclaim responsibility for any injury to people or property resulting from any ideas, methods, instructions or products referred to in the content.